Catalytic performance of zirconia-supported oxides (Nb_2O_5, SiO_2 and WO_3) in ethanol upgrading: influence of acid-base properties

Desempenho catalítico de óxidos suportados em zircônia (Nb_2O_5, SiO_2 e WO_3) no beneficiamento de etanol: influência das propriedades ácido-básicas

DOI:10.34117/bjdv8n8-189

Recebimento dos originais: 21/06/2022
Aceitação para publicação: 29/07/2022

Mathilde Marie Catherine Laird
Doutora em Química pela École Nationale Supérieure de Chimie de Montpellier
Institution: Universidade Federal do Rio de Janeiro (UFRJ)
Address: Cidade Universitária, CEP: 21941-972, Rio de Janeiro
E-mail: Mathilde.llp@gmail.com

Victoria Gonçalves Ferreira Pereira
Doutoranda em Engenharia Química pela Universidade Federal do Rio de Janeiro (UFRJ)
Institution: Universidade Federal do Rio de Janeiro (UFRJ)
Address: Cidade Universitária, CEP: 21941-972, Rio de Janeiro
E-mail: victoria@peq.coppe.ufrj.br

Marcos Anacleto da Silva
Doutorado em Ciência e Tecnologia de Polímeros pela Universidade Federal do Rio de Janeiro (UFRJ)
Institution: Universidade Federal do Rio de Janeiro (UFRJ)
Address: Cidade Universitária, CEP: 21941-972, Rio de Janeiro
E-mail: anacleto@peq.coppe.ufrj.br

Felipe da Silva Lopes
Pós-graduando em Gestão da Segurança dos Alimentos e Qualidade Nutricional pelo Instituto Federal do Rio de Janeiro (IFRJ)
Institution: Instituto Nacional de Tecnologia (INT)
Address: Rio de Janeiro, CEP: 20081-312, Brasil
E-mail: felipeslopes@mail.com

Henrique Poltronieri Pacheco
Doutor em Engenharia Química pela Universidade Federal do Rio de Janeiro (UFRJ)
Institution: Universidade Federal do Rio de Janeiro (UFRJ)
Address: Cidade Universitária, CEP: 21941-972, Rio de Janeiro
E-mail: henrique@peq.coppe.ufrj.br

Clarissa Perdomo Rodrigues
Doutora em Engenharia Química pela Universidade Federal do Rio de Janeiro (UFRJ)
Institution: Instituto Nacional de Tecnologia (INT)
Address: Rio de Janeiro, CEP: 20081-312, Brasil
E-mail: clarissa.rodrigues@int.gov.br

Fabio Souza Toniolo
Doutor em Engenharia Química pela Universidade Federal do Rio de Janeiro (UFRJ)
Institution: Universidade Federal do Rio de Janeiro (UFRJ)
Address: Cidade Universitária, CEP: 21941-972, Rio de Janeiro, Brasil
E-mail: toniolo@peq.coppe.ufrj.br

ABSTRACT
We present a study of ethanol upgrading on zirconia-based metal oxides including commercial SiO_2/ZrO_2, WO_3/ZrO_2, pure zirconia catalysts and a Nb_2O_5/ZrO_2 catalyst obtained by wet impregnation. Chemical composition, crystallographic features, textural and acid-base properties (NH_3 and CO_2 temperature programmed desorption) were determined. Reactivity of the catalysts was investigated by temperature programmed surface reaction and isothermal catalytic tests. Catalyst performance was strongly dependent on the acid-base properties which favored the ethanol dehydration to ethylene. All modified zirconia-base catalysts yielded C3 and C4 compounds above 623 K. This study consequently emphasizes the preponderant role of both acid and basic site in the formation of higher products from ethanol.

Keywords: ethanol conversion, niobia, metal oxide catalyst, acid-base properties, deactivation.

RESUMO
Este trabalho apresenta um estudo sobre o beneficiamento de etanol empregando óxidos metálicos à base de zircônia incluindo SiO_2/ZrO_2 comercial, WO_3/ZrO_2, zircônia pura e Nb_2O_5/ZrO_2 obtido por impregnação úmida. A composição química e as propriedades cristalográficas, texturais e ácido-básicas (dessorção de NH_3 e CO_2 a temperatura programada) foram determinadas. A reatividade dos catalisadores foi investigada por reação superficial a temperatura programada e testes catalíticos isotérmicos. O desempenho do catalisador foi fortemente dependente das propriedades ácido-básicas que favoreceram a desidratação de etanol a etileno. Todas os catalisadores de zircônia modificada produziram compostos C3 e C4 acima de 623 K. O presente estudo destaca o papel preponderante dos sítios ácidos e básicos na formação de produtos superiores a partir do etanol.

Palavras-chave: conversão de etanol, nióbia, catalisador de óxido metálico, propriedades ácido-básicas, desativação.

Graphical abstract

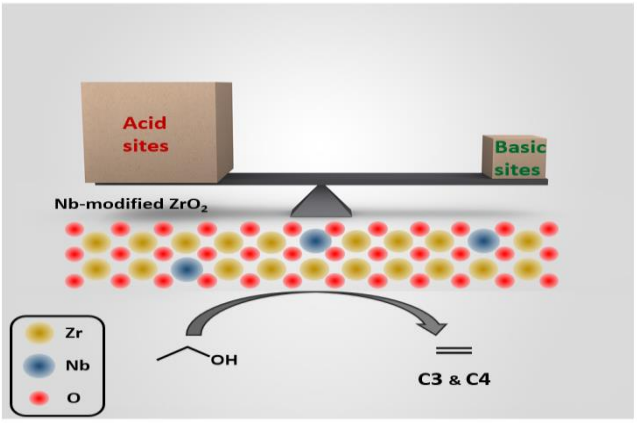

1 INTRODUCTION

Ethanol conversion into higher products receives significant attention in both industrial and academic fields. As an inexpensive commercial product, possibly convertible into products that can gradually replace several existing petrochemicals, ethanol is ranked among the top ten opportunities for biorefineries [1]. Ethanol-derived compounds include ethylene, acetic acid, ethyl acetate, 1,3-butadiene, propene, acetone, 1-butanol, acetaldehyde, large hydrocarbons, aromatics, among others [2–4]. As the production of such higher- added value chemicals is usually competitive in the same system, it is crucial to further understand the adsorption phenomena and surface chemistry that take place on the catalyst, especially regarding the critical reaction steps determining selectivity and rate-limiting steps.

To date, most of the catalysts studied for the ethanol conversion to ethylene are based on alumina or zeolites. The acidic properties of these catalysts were proved to have a key role on their reactivity [4, 5]. In the 1980s, a new catalyst named “Syndol” was commercially released. This catalyst was composed of $MgO\text{-}Al_2O_3/SiO_2$ and allowed for 99 % selectivity towards ethylene and ethanol conversion of 99.8 %; however, temperatures as high as 883 K were still required [6]. Since then, several metal oxide catalysts were studied, with alumina-based materials revealing the most interesting results [2, 5, 7]. Indeed, up to 99 % ethanol conversion and 99 % ethylene selectivity could be achieved between 623 K and 713 K [7]. An HZMS-5 zeolite catalyst also enabled 98 % conversion and 95 % ethylene selectivity at 573 K [5]. Zeolite-derived catalysts, which are now the most commonly used for ethanol dehydration to ethylene, could reach 99 %

ethanol conversion and 99 % selectivity at 513 K [7]. Nevertheless, the hydrothermal instability of the zeolites is a limiting factor for their use as catalyst-of-choice. [8]

Heavier products can also be produced by ethanol upgrading, including acetone, acetic acid, ethyl acetate, propylene, butenes, 1,3-butadiene, and 1-butanol [2, 9–16]. 1,3-Butadiene synthesis over metal oxides, especially MgO/SiO_2 catalysts, is of particular interest [17–20]. Proper tuning of the acid-base properties allows for dehydrogenation/condensation reaction steps of the catalytic cycle of 1,3-butadiene production to be favored, since several competing routes take place in ethanol reacting systems (see Section 3.2 for further discussion).

Among the different oxides used for ethanol upgrading, zirconia has been described as a promising material. In 2016, Yu *et al*. [21] investigated the formation of ethylene and 1,3-butadiene from ethanol, assuming that the high reactivity of the zirconia is related to its acid-base properties. The importance of such features was also supported by Rodrigues *et al*. [22], who studied the formation of acetone from ethanol, and characterized the acidity and basicity of these sites by CO_2 temperature-programed desorption (TPD) and pyridine adsorption. Later, the influence of the thermal treatment temperature of zirconia on the catalytic performance to convert ethanol to propylene was assessed [23, 24]. Despite these studies probing the acid-base properties of the catalyst, few correlations were found between these and the catalytic performance. Silica-zirconia mixed oxides were also analyzed for the conversion of ethanol to ethylene [25] and to 1,3-butadiene [26]. The Zr-O-Zr bond was found to be crucial, as it determined the acid-base properties of the catalyst.

Transition metals-doped zirconia was investigated as well. The influence of tungsten oxide on zirconia has been better understood thanks to the works of Houalla's [27] and Busca's groups [28]. Both concluded that the presence of strong acid sites, introduced *via* tungsten oxide, enhanced the catalytic performance towards the dehydration of the alcohol to alkenes. On the other hand, niobium-derived oxide catalysts were scarcely studied [29, 30]. In 1986, Iwasawa and co-workers [31] discovered the efficiency of niobium pentoxide in ethanol dehydrogenation/dehydration. Lewis acid sites were assumed to be a key point of the transformation of ethanol to ethylene and diethyl ether over a niobium monolayer catalyst supported on silica. However, no characterization of these sites was performed. At a later stage, Brandão *et al*. [32] reported the capacity of mesoporous niobium-silica to convert alcohols into their corresponding olefins or ethers. With ethanol as reactant, a conversion of 98 % and a selectivity of 97 %

towards ethylene at 523 K was reported. Zhu's group [33] also published a study related to ethanol conversion into ethylene, acetaldehyde and diethyl ether on niobium-containing mesoporous silica. They characterized acidity and basicity of the materials and reaffirmed the necessity of both types of sites in the ethanol conversion to higher products over niobium-doped silica.

Catalysis, management of local resources, and the use of renewable raw materials are part of the green chemistry principles and key points for chemistry development [34] . As Brazil is one of the biggest producers of ethanol [35] and possesses more than 90 % of worldwide niobium resources [36], our group investigated the transformation of ethanol giving particular attention to niobium catalysts. In this paper, we aim at investigating the catalytic activity of metal oxides that have not been extensively employed yet in ethanol conversion. Focus will be given to the catalytic behavior of zirconia doped with WO_3, SiO_2 and Nb_2O_5 in the ethanol conversion into higher products. Additionally, we suggest correlating the physicochemical properties of the materials with the catalytic performance and selectivity to products.

2 EXPERIMENTAL

2.1 CATALYSTS SYNTHESIS

NORPRO Saint-Gobain commercial zirconia was used as support. This monoclinic zirconia was thermally treated at 723 K for 12 h and then sized to a particle range below 149 µm. The obtained material was used for the synthesis of the niobium-doped zirconia catalyst. This zirconia was also used as reference for raw zirconia materials.

The niobium-supported catalyst was synthesized as follows: a precursor of niobium ammonium oxalate $(NH_4)[NbO(C_2H_4)_2(H_2O)_2].3H_2O$ (from CBMM) was chosen as niobium source. The zirconia support and the niobium ammonium pentoxide precursor were dried overnight. The required quantity of dried niobium precursor was diluted in distillated water in order to obtain a 3.5 wt.% Nb_2O_5/ZrO_2 catalyst. The niobium solution was prepared with a volume of at least the porous volume of the quantity of support to be impregnated (based on the N_2 physisorption data). For our catalyst, 2 g of zirconia were impregnated with a solution of 0.186 g of $(NH_4)[NbO(C_2H_4)_2(H_2O)_2]$ in 1.2 mL of distilled water. The obtained solution was impregnated until the wet point, then dried at 403 K for at least 30 min and impregnated again until depletion of the solution.

The impregnated zirconia was finally thermally treated in static air at 673 K for 6 h at a temperature rate of 10 K·min^{-1}.

As an effort to benchmark our findings, two commercial catalysts were also tested: a 10 wt.% WO_3/ZrO_2 and a 3.5 wt.% SiO_2/ZrO_2 from MEL Company, both thermally treated in air at 723 K for 12 h at a temperature rate of 10 K·min^{-1}.

2.2 CATALYST CHARACTERIZATION

Chemical composition of the zirconia-supported oxides was determined by X-ray fluorescence (XRF) in a Rigaku RIX 3100 with rhodium target tube operated at 4 kW. Textural properties were investigated by N_2 physisorption at 77 K with a Micromeritics ASAP 2020. All samples were dried under vacuum at 673 K for 24 h and then the adsorption and desorption isotherms were collected. Pore size distribution and the average pore size were obtained by the BJH method from the desorption isotherm. Specific surface area was obtained by the BET method.

X-ray diffraction (XRD) patterns were recorded in a Bruker diffractometer, D8 Advance, with copper radiation (CuKα, λ=1.5418 Å) within a Bragg angle range of 10° ≤ 2θ ≤ 90°, with 0.05° step size and counting time of 2 s per step. The crystallite sizes were calculated by the Scherrer equation:

$$\tau = \frac{K\lambda}{\beta \cos\theta} \qquad (1)$$

where τ is the average particle size in Å, θ is the Bragg angle, λ is the wavelength in Å, β is the full width at half maximum (FWHM) in rad, and K is the form factor (K = 0.89).

Acid site density of the samples was determined by NH_3-TPD, which was carried out in a fixed-bed, U-shaped quartz reactor (12 mm i.d.) with a 100 mg catalyst bed under atmospheric pressure. A thermocouple was placed in contact with the reactor wall at the bed height. The sample was dried at 403 K in He (60 mL·min^{-1}) for 30 min. Ammonia adsorption was held under 4 vol.% NH_3/He (60 mL·min^{-1}) at room temperature for 30 min, and then the system was purged with helium (60 mL·min^{-1}) for 1 h. Desorption was followed from room temperature up to 873 K at 10 K·min^{-1} under helium (60 mL·min^{-1}). Desorption gases were analyzed online by a Balzers-Pfeiffer mass spectrometer. NH_3-TPD profiles were deconvoluted in three Gaussian curves with maxima at temperatures

below 473 K, between 473-623 K and above 623 K, ascribed to weak (W), medium (M) and strong (S) acid sites, respectively [37].

Similarly, basic site density of the samples was determined by CO_2-TPD, which was carried out in the same unit configuration described above and employing the same mass spectrometer. The sample was first dried for 30 min at 403 K with a 60 mL·min^{-1} helium flow. CO_2 adsorption was conducted at room temperature for 30 min, and the system was purged with helium for 1 h. Desorption was followed from room temperature up to 873 K at 10 K·min^{-1} under helium flow. All gases were used at 60 mL·min^{-1}. CO_2-TPD profiles were deconvoluted in three Gaussian curves with maxima at temperatures below 400 K, between 400-580 K and above 580 K, corresponding to weak (W), medium (M) and strong (S) basic sites, respectively, as described elsewhere [38, 39].

Post-reaction thermo-gravimetric analysis (TGA) of the Nb_2O_5/ZrO_2, SiO_2/ZrO_2 and WO_3/ZrO_2 samples were performed on a TG-DTA Rigaku Thermo PlusTG8120 under 20% O_2/N_2 flow and heating rate of 10 K·min^{-1} from room temperature up to 1273K. The mass losses were corrected considering the dilution rate (1:10) used in the catalyst preparation for the isothermal test, *vide infra*.

2.3 CATALYTIC EVALUATION

2.3.1 Temperature Programmed Surface Reaction (TPSR) of Ethanol

Ethanol TPSR was carried out in a fixed-bed, U-shaped quartz reactor (12 mm i.d.) loaded with 100 mg of catalyst under atmospheric pressure. All samples were pretreated at 403 K for 30 min under a 60 mL·min^{-1} helium flow. A thermocouple was placed in contact with the reactor wall at bed height. Ethanol was injected into the reactor by flowing helium at 60 mL·min^{-1} through a saturator containing ethanol and held at 273 K by a thermal bath. According to Antoine's equation, a stream of 1.55 vol% EtOH/He was achieved. TPSR tests were then performed from room temperature up to 873 K, at heating rate of 10 K·min^{-1}, and kept at this temperature for 20 min. The products were analyzed online with a Balzers-Pfeiffer mass spectrometer equipped with an electronic impact ionizer. The simultaneously followed fragments were: ethanol (m/e = 31), acetaldehyde (m/e = 29), ethane (m/e = 27), ethylene (m/e = 26), diethyl ether (m/e = 59), ethyl acetate (m/e = 61), acetone (m/e = 58), 1-butanol (m/e = 56), crotonaldehyde (m/e = 70), 1,3-butadiene (m/e = 54) and carbon dioxide CO_2 (m/e = 44).

2.3.2 Catalytic Tests

Catalytic tests were performed in a fixed bed glass reactor (U shaped) at 623 K, 673 K and 723 K under atmospheric pressure. 40 mg of the samples were diluted in 400 mg of silicon carbide to avoid the formation of hot spots throughout the catalyst bed. The samples were then pretreated under He flow (80 mL·min^{-1}) at 473 K for 1 h. A 5% ethanol/He stream (80 mL·min^{-1}) was fed into the reactor and the reaction was performed for 90 min at each temperature. The outlet composition was monitored by online gas chromatography, employing a GC Varian CP 3380 chromatograph, equipped with a PoraPLOT Q column (30 m, 0.53 mm i.d.), a thermal conductivity detector (TCD) and a flame ionization detector (FID). The results were recorded as an average of three injections at each temperature. To check for catalyst deactivation, another injection was recorded at 623 K after cooling down the system from 723 K.

Ethanol conversion (X) and product selectivities (S) were calculated as in Equations (2) and (3), respectively, where $F_{ethanol,in}$ and $F_{ethanol,out}$ refer to the molar flow of ethanol at the reactor inlet and outlet, respectively, F_i refers to the molar flow of the product i,and F_p is the total molar flow of products.

$$X\ (\%) = \frac{F_{ethanol,in} - F_{ethanol,out}}{F_{ethanol,in}} x100 \qquad (2)$$

$$S_i(\%) = \frac{F_i}{F_p} x100 \qquad (3)$$

3 RESULTS AND DISCUSSION

3.1 CATALYST CHARACTERIZATION

Table 1 presents the chemical compositions of the catalysts by XRF, which confirmed the purity of the starting zirconia material. Hence, the detected hafnium oxide percentage is related to the extraction procedure of the zirconium oxide; others oxides are negligible. In addition, the 3.7 wt.% of niobium recorded on zirconia evidences a complete incorporation of the former into the ZrO_2 structure. Indeed, the niobium amount is close to the 3.5 wt.% nominal value. Experimental values of the commercial sample are consistent.

The results from the physisorption analysis are displayed in Table 1. All catalysts present a hysteresis loop attributed to the presence of mesopores. The zirconia support presents specific surface area of 103 m^2·g^{-1} with a wide distribution of pore diameter ranging between 3 and 50 nm (maximum at 5 nm). The impregnation of the niobium

solution on the zirconia support led to a decrease of the specific surface area to 61 $m^2 \cdot g^{-1}$. This result is consistent with the formation of niobia clusters, occupying the free pore surface [40]. It is worth noting that both 3.5 wt.% SiO_2/ZrO_2 and 10 wt.% WO_3/ZrO_2 catalysts are commercial samples and do not come from the same zirconia support. Their specific surface area is similar to the raw zirconia support with an equally high pore size distribution.

Table 1: Chemical composition and structural properties

Catalyst	**Chemical Composition / wt.%**	**A_{BET} / $m^2 \cdot g^{-1}$**	**Pore Volume / $cm^3 \cdot g^{-1}$**	**Mean Pore Size / Å**	**Mean Crystallite Size / Å**
ZrO_2 (100)	97.6 *	104	0.29	89	89
Nb_2O_5/ZrO_2 (3.5/96.5)	3.7/95.3 **	61	0.25	130	129
SiO_2/ZrO_2 (3.5/96.5)	3.8/96.2	96	0.28	85	56
WO_3/ZrO_2 (10/90)	10.9/89.1	108	0.38	114	70

** ZrO_2 sample presented 2.4 wt.% of HfO_2*
** Nb_2O_5/ZrO_2 sample presented 1.0 wt.% of HfO_2

Figure 1 shows the XRD profiles of the catalysts. Pure zirconia support presents characteristic peaks of monoclinic ZrO_2 phase (m-ZrO_2, COD 9016714, full blue circle in Figure 1). Nb_2O_5/ZrO_2 also presents monoclinic ZrO_2 phase; however, diffraction peaks related to the niobia phase could not be identified. This either suggests that Nb_2O_5 is highly dispersed over ZrO_2 surface, obtaining small crystallites that could not be detected by XRD, or that the Nb_2O_5 phase is amorphous. In fact, the Nb_2O_5 framework is quite complex and presents polymorphism. The phase transition temperature depends on precursor, impurities and thermal treatment conditions. Consequently the temperature range of phase transition is slightly variable [41]. Nonetheless, the transition from amorphous Nb_2O_5 to orthorhombic and pseudohexagonal phases is commonly observed around 773 K. In this work, Nb_2O_5 was treated at 673 K, which suggests that the impregnated material may be amorphous. SiO_2/ZrO_2 presented characteristic peaks of cubic ZrO_2 phase (c-ZrO_2, COD 1521753, full pink diamond in Figure 1). Diffraction patterns related to SiO_2 were not identified, inferring an amorphous silica phase, which is consistent with the literature [42]. The WO_3/ZrO_2 profile evidenced the presence of both monoclinic and cubic ZrO_2 phases in this catalyst. No diffraction peaks related to WO_3 were identified as observed in similar samples [43].

Figure 1-X-ray diffraction profiles of the catalysts. m-ZrO_2, COD 9016714 (full blue dot ●); c-ZrO_2, COD 1521753 (full pink diamond ♦).

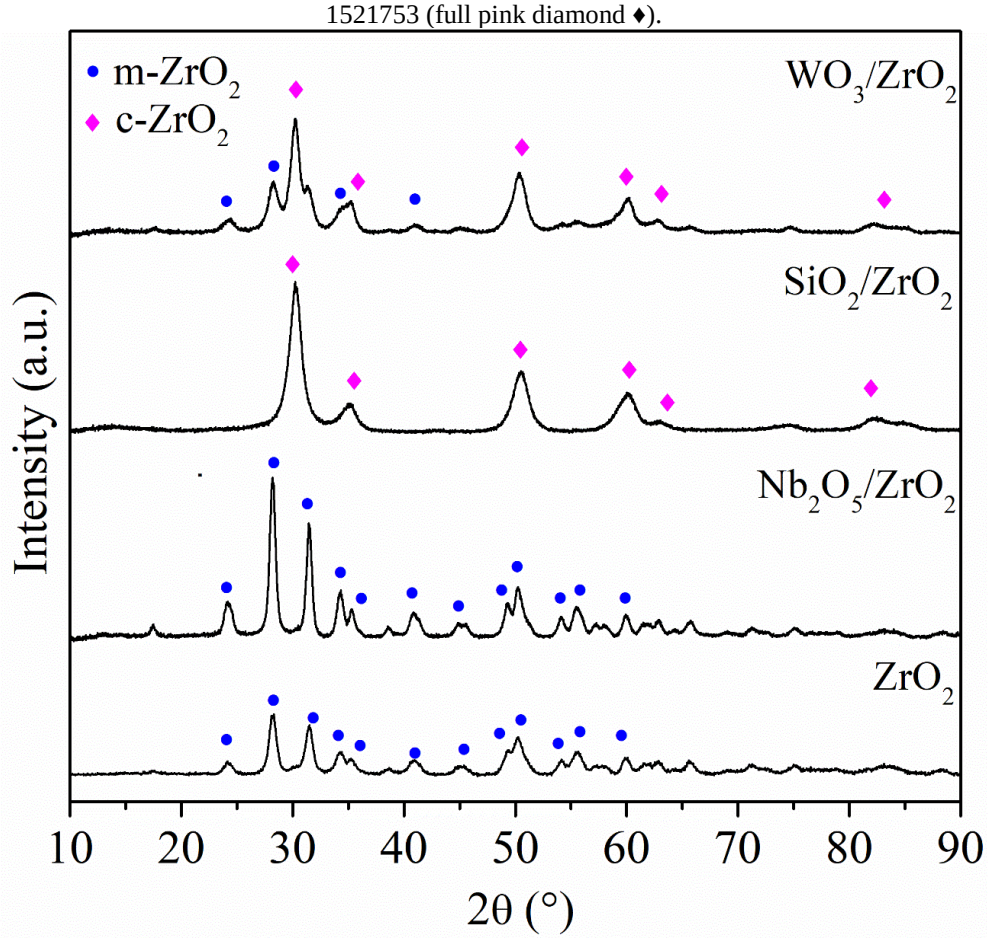

Figure 2 presents the ammonia desorption profiles determining acid site density (numeric results shown in Table 2) and estimating the relative acid site strength. The assumption that ammonia bonded to stronger acid sites desorbs at higher temperatures was considered. The acid sites that are referred to as weak are related to desorption peaks that show a maximum at temperatures lower than 473 K; those between 473 K and 623 K are referred to as medium; and those above 623 K are referred to as strong acid sites. This study does not quantitatively characterize the strength of the acid site but proposes a qualitative study based on the definition previously cited and used in the literature [37].

Figure 2- NH_3 TPD: (a) ZrO_2 (b) Nb_2O_5/ZrO_2 (c) SiO_2/ZrO_2 (d) WO_3/ZrO_2. From 873 K on an isothermal regime is applied.

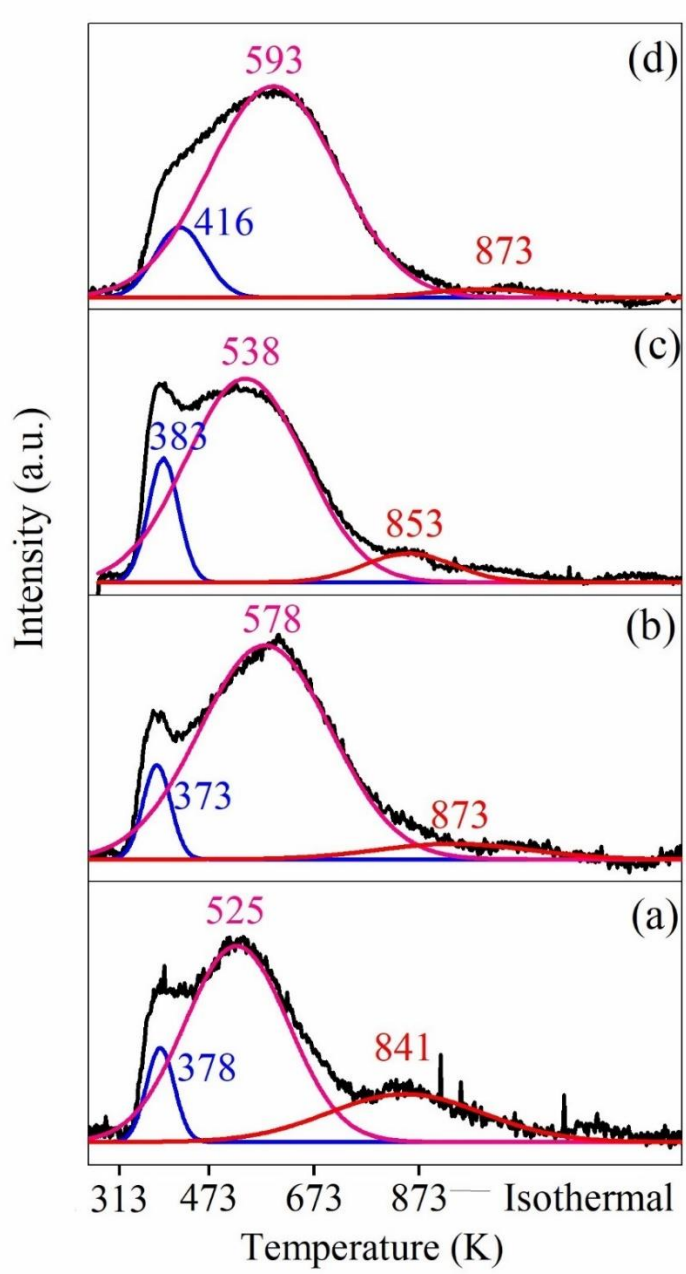

ZrO_2 is a significantly ionic oxide, partly composed of Zr^{+4} cations. It is thus characterized by medium Lewis acidity, significant surface basicity and very low Brønsted acidity [44]. Figure 2 shows that the ZrO_2 support presents weak, medium and strong acid sites. As observed in Table 2, medium and strong acid sites are predominant, with the total acidity being in the range generally observed for zirconia [45–48]. Despite an inherent acidity relatively low for pure Nb_2O_5 [49–51], the doping of the support with niobia generally increases the total acid sites density [49, 52, 53]. The increase in acidity from 285 to 444 $\mu mol \cdot g^{-1}$, observed after niobium doping, was thus expected. Yang *et al*.

[51] reported a similar niobia-doped zirconia material with a total acidity of around 180 $\mu mol \cdot g^{-1}$. The material obtained in our study presents higher acidity when compared to similar materials. Nonetheless, it can be observed that the density of strong acid sites decreased, probably due to the replacement of strong sites by medium ones related to the covering of active zirconia sites by niobium species [27]. Onfroy *et al.* [27, 54, 55] also observed an increase in acid sites in supported niobia catalysts. They reported the existence of two types of acid sites on zirconia-supported niobia catalysts: Lewis acid sites, which decreased in number, but increased in strength with niobium loading; and Brønsted acid sites, which followed the niobium loading. Thus, the Nb_2O_5 addition increased the catalyst acidity, but also changed the sites' strength [27, 54, 55]. SiO_2/ZrO_2 and WO_3/ZrO_2 exhibited the highest density of acid sites of around 700 $\mu mol \cdot g^{-1}$. It is central to emphasize that these are commercial samples that were not originated from the ZrO_2 support. Accordingly, XRD analysis (Figure 1) showed the presence of cubic ZrO_2 crystalline phase in these samples, and then the acid properties may be different from monoclinic ZrO_2 [56]. Still, the addition of WO_3 may have increased acid site density. Onfroy *et al*. [43, 57] as well as Busca's group [28] reported an increase in acidity with tungsten addition to zirconia. Such behavior is similar to zirconia-supported niobia: Lewis acid sites decreased in number with the loading of tungsten but increased in strength. Additionally, strong Brønsted acid sites appeared and increased linearly with tungsten loading. In this work, WO_3/ZrO_2 presented mostly medium strength acid sites with total acidity slightly superior to a similar material described in the literature [58]. SiO_2/ZrO_2 revealed the largest acid site density and mostly medium strength acid sites. As Gervasini and Auroux [59] already reported on the behavior of acid sites on pure silica, the high acidity on the mixed SiO_2/ZrO_2 oxide is not surprising and is on the range of the value previously described [47, 48]. On the other hand, although the observed acidity in the catalysts in this study is consistent with the literature, the concentration of acid sites is moderate in comparison to values observed for metal oxides doped with phosphorous [58], sulfates [60], or higher value transition metals, including ruthenium, gadolinium, and nickel [61–63].

Figure 3 shows the CO_2 desorption profiles. The basic site density quantification is presented in Table 2. The basic sites, which are referred to as weak, are related to desorption peaks that show a maximum at temperatures lower than 400 K; those between 400 K and 580 K are referred to as medium; and those above 580 K are referred to as strong basic sites. Here again, this study do not quantitatively characterize the strength of

the basic site but propose a qualitative study based on the previous definition and used in the literature [38, 39].

Figure 3- CO_2 TPD: (a) ZrO_2 (b) Nb_2O_5/ZrO_2 (c) SiO_2/ZrO_2 (d) WO_3/ZrO_2. From 873 K on an isothermal regime is applied.

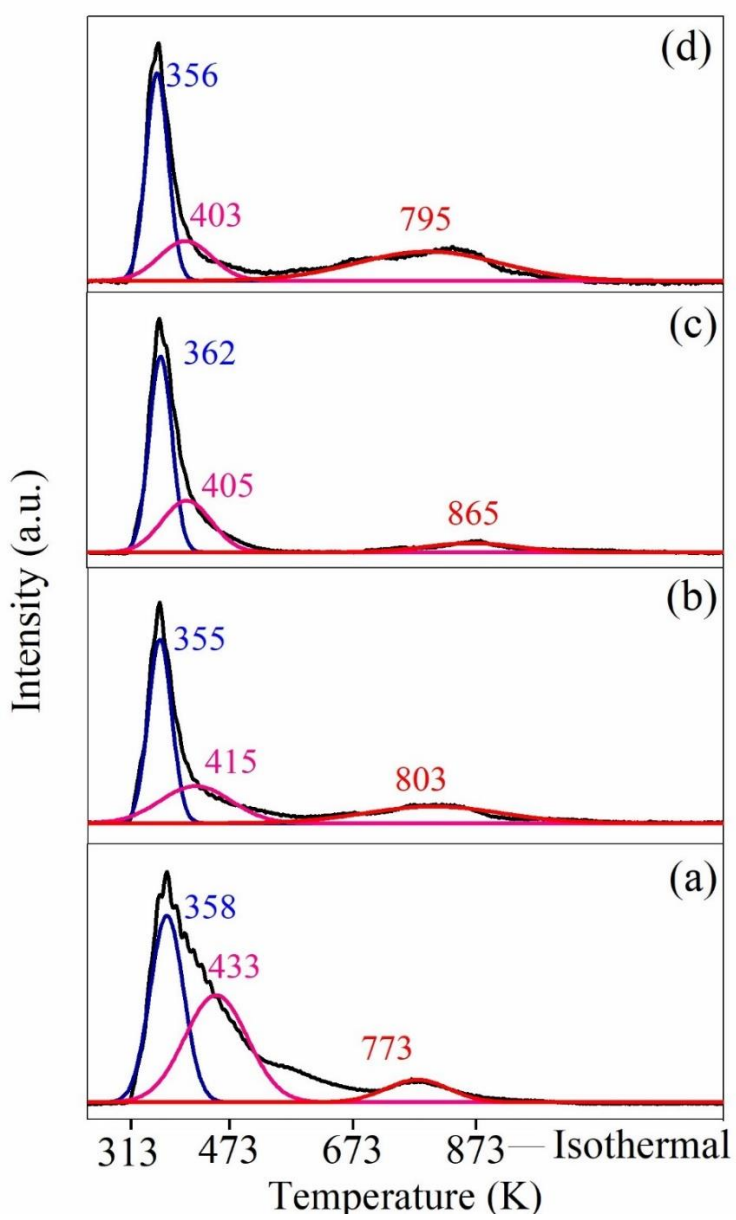

According to Figure 3 and Table 2, all catalysts presented weak, medium and strong basic sites; in any case, weak and medium strength basic sites are mainly observed. According to previous studies [64, 65], ZrO_2 is known as a bifunctional catalyst with both weak acid and basic sites. Interestingly, the amount of basic site observed for the zirconia support is 30-fold lower than previously described in the literature [45]. The addition of Nb_2O_5 to ZrO_2 decreased the number of basic sites, which can be explained by the partial

neutralization of ZrO_2 basic sites during the impregnation of Nb_2O_5 [66]. Concerning the WO_3/ZrO_2 catalyst, WO_3 contributed more to the acidity than to the basicity, resulting in a lower number of basic sites [30, 31]. Here, once again, the proportion of basic site is 50-fold lower than previously described for similar materials [67]. Much higher basic site density can be obtained when doping the metal oxide support with a transition metal such as copper or zinc [68, 69].

Table 2- Acid and basic sites density.

Catalyst	Basic sites density / µmol g_{cat}^{-1}				Acid sites density / µmol g_{cat}^{-1}			
	W	M	S	Tot	W	M	S	Tot
ZrO_2	6	10	2	18	25	161	69	285
Nb_2O_5/ZrO_2	4	2	2	8	35	378	32	444
SiO_2/ZrO_2	6	3	1	10	95	604	64	763
WO_3/ZrO_2	2	1	1	4	73	571	19	663

W: weak; M: medium; S: strong; Tot: total.

3.2 CATALYTIC EVALUATION

3.2.1 TPSR of Ethanol

Zirconia-supported catalysts were tested in transient experiments of ethanol conversion with EtOH/He = 1.55 vol%. Particular focus is given to ethylene and to diethyl ether, as the latter is an important byproduct of ethylene formation [7, 70–72]. Acetone, crotonaldehyde, 1,3-butadiene and 1-butanol were also assessed. Figure 4 presents different reaction pathways mentioned in the literature for 1-butanol, 1,3-butadiene and acetone [10, 13, 78, 14, 15, 37, 73–77]. Those well-accepted by the community are presented in black, while alternative paths are drawn in grey; however, those routes are still subject to an ongoing debate in the scientific community, especially regarding aldol-containing routes and the several hydrogenation steps [15, 16].

Dehydration to ethylene and to diethyl ether takes place according to steps 1 and 2 in Figure 4, respectively. Ethanol dehydration is known to usually occur on acid-base pairs of metal oxides with strong acidic character [2, 5, 7]; nevertheless, olefin formation requires higher temperatures to surpass its high activation energy when compared to its ether counterpart [76]. Consequently, diethyl ether formation is favored at lower temperatures [70]. 1-Butanol, 1,3-butadiene, acetone, CO_2 and crotonaldehyde are also produced by ethanol upgrading and are competing routes to the dehydration products, since steps 3 and 4 in Figure 4 also compete for ethanol molecules in the feed stream.

Although several reports suggest that the central mechanism for the upgrading of ethanol to 1-butanol is via direct dimerization (Figure 4 - step 21 and 23) [77, 79], the most accepted reaction pathway involves a more convoluted reaction path [15, 73, 76, 80–85].

Figure 4- Reaction pathways for different ethanol upgrading products; well-accepted routes represented in black, alternative routes in grey.

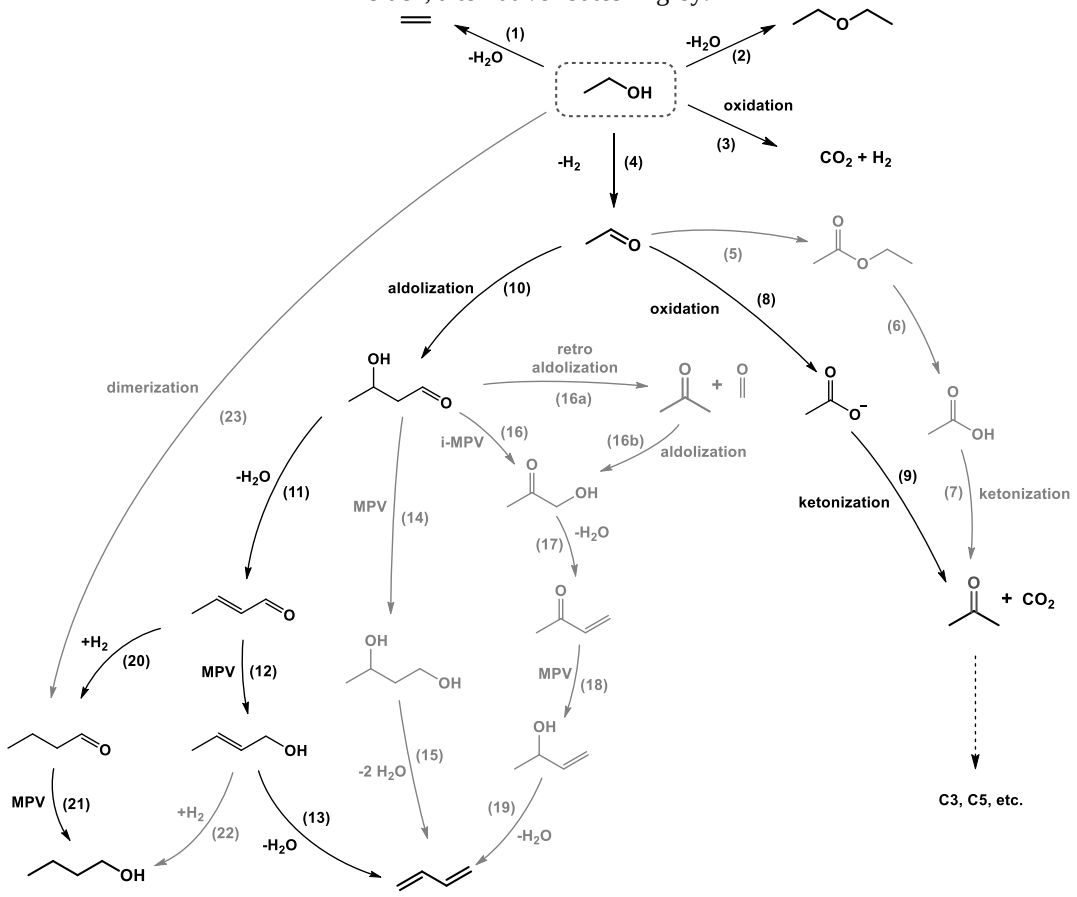

The formation of 1-butanol occurs via dehydrogenation of ethanol to acetaldehyde followed by an aldol condensation step to 3-hydroxybutyraldehyde, dehydration to crotonaldehyde, and hydrogenation to butyraldehyde and 1-butanol (Figure 4 - step 4, 10, 11, 20 and 21). This reaction route is known as the Guerbet reaction and it is not under the scope of this paper to delve further into its intricacies. Acid-base pair sites with high density of basic sites and with very particular topology and defect structures have been shown to be critical to the formation of the aldol condensation product [15, 73, 76, 81]. Similarly, this aldolization step on acid-base pair sites appeared as a key point to the 1,3-butadiene formation from ethanol (Figure 4 - step 10). Even though this reaction pathway is also still subject to debate [13, 19, 26, 37, 73–75], all routes encompass acetaldehyde and 3-hydroxybutyraldehyde as intermediates. The most accepted reaction pathway,

referred to as Gorin-Jones route, proposes the formation of acetaldehyde by dehydrogenation on basic or redox sites prior to aldol condensation on an acid-base pair site to form 3-hydroxybutyraldehyde (Figure 4 - step 4 and 10). The aldol is then dehydrated to crotonaldehyde on acid sites, converted into 2-butenol by Meerwein-Ponndorf-Verley reaction (MPV) and dehydrated again to 1,3-butadiene (Figure 4 - step 11, 12 and 13) [19, 86]. However, Dussol *et al*. [74] supported an alternative reaction route inspired by Inoué *et al*. [87], involving methyl-vinyl-ketone as an intermediate instead of crotonaldehyde (Figure 4 - step 4, 10 and 16-20). Despite this questioning, crotonaldehyde was followed as a possible intermediate of 1-butanol and 1,3-butadiene. Acetone production, as one of the products of ethanol upgrading, was also followed in this study. The widely accepted reaction path involves the oxidation of the acetaldehyde intermediate prior to ketonization [22, 64] (Figure 4 steps 8 and 9).

Figure 5 presents the ethanol TPSR profiles observed for ZrO_2, Nb_2O_5/ZrO_2, SiO_2/ZrO_2 and WO_3/ZrO_2. All zirconia-doped catalysts exhibited catalytic activity starting around 573 K and an ability to yield C2 to C4 products. Ethanol is totally converted between 543 K and 723 K (Figure 5a). According to this observation, it can be concluded that all catalysts have a temperature of half conversion of ethanol around 633 K, except for the 10 wt.% WO_3/ZrO_2 catalyst, whose temperature is lower (around 593 K), probably due to the high acidity of the tungsten-modified zirconia. Ethylene appeared as one of the main products of reaction over all catalysts, resulting from the dehydration of ethanol over acid sites of the metal oxides [7]. In Figure 5b, the WO_3/ZrO_2 and SiO_2/ZrO_2 catalysts, presenting the highest acidity (763 and 663 $\mu mol \cdot g_{cat}^{-1}$, respectively), exhibited peaks of ethylene production at low temperatures (613 K and 653 K, respectively), while the other catalysts quickly reached a plateau at around 673 K. The WO_3/ZrO_2 catalyst revealed both the lowest temperature of half ethanol conversion and the lowest temperature of the peak of ethylene production (613 K). This high activity probably results from the observed large quantity of acid sites.

Figure 5: Ethanol (m/e = 31) conversion (a) and ethylene (m/e = 27) production (b) profiles as a function of temperature on different catalysts.

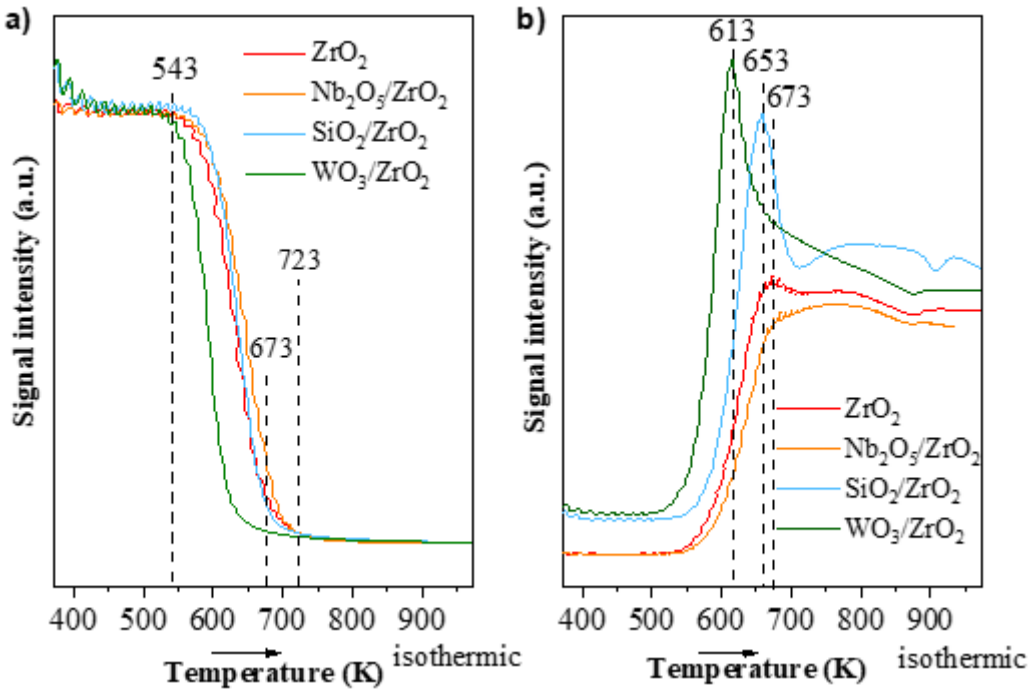

Figure 6 presents the TPSR profiles of CO_2, acetone, diethyl ether, acetone, crotonaldehyde, 1,3-butadiene and 1-butanol over the four analyzed catalysts. As expected [7], diethyl ether is formed at lower temperatures than ethylene for all four materials (with peaks at 633 K, 653 K, 633 K and 578 K for ZrO_2, Nb_2O_5/ZrO_2, SiO_2/ZrO_2 and WO_3/ZrO_2 respectively). It is noteworthy that the diethyl ether peaks appeared at lower temperature for the WO_3/ZrO_2 compared to the other catalysts. This can be explained again by the important quantity of acid sites in this oxide. In addition, it is relevant to note that acetone and CO_2 started to desorb at the same temperature (around 673 K). This observation suggests that the ketonization reaction [22, 64], involved in the acetone route, is responsible for part of the CO_2 production (Figure 4 - steps 9 and 7). The presence of redox sites on zirconia enables ethanol and acetaldehyde to be oxidized and basic sites promote the ketonization reaction (Figure 4, steps 5-9). Interestingly, the CO_2 profile did not strictly follow the acetone one. Total oxidation of ethanol (Figure 4, step 3) has been reported over zirconia and zirconia-modified materials [78], due to the redox sites present on zirconia [88]. As the oxidation reaction of ethanol is endothermic, a larger quantity of CO_2 is expected at high temperature, as observed in Figure 6a at 673 K [89].

Figure 6: Ethanol TPSR on a) ZrO_2 b) Nb_2O_5/ZrO_2 c) SiO_2/ZrO_2 d) WO_3/ZrO_2: composition profiles.

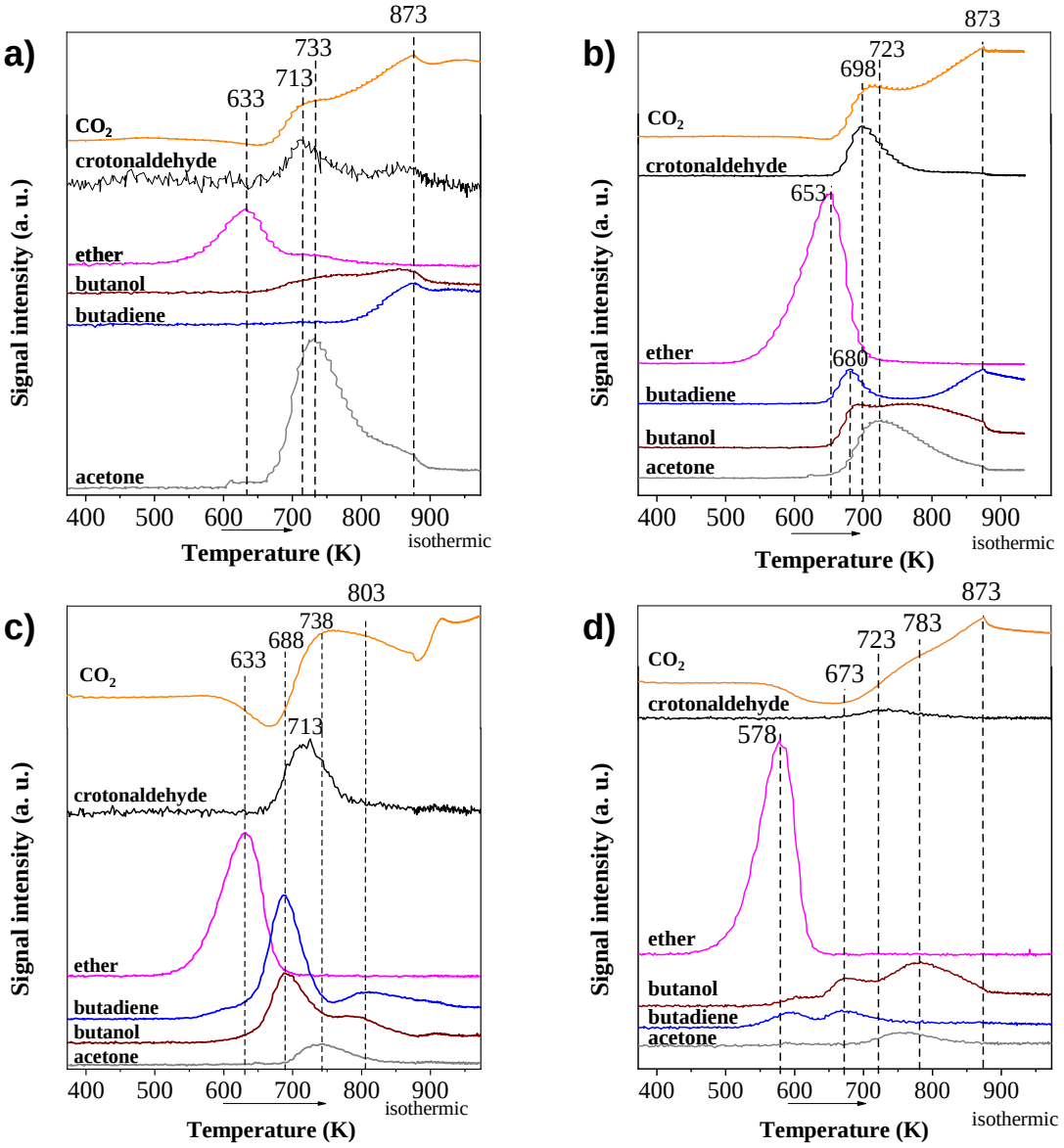

TPSR of ethanol on ZrO_2 in Figure 6a evidences the formation of 1-butanol, crotonaldehyde, acetone and CO_2 starting at 673 K. The generation of these compounds is simultaneous to the observed plateaus in ethylene production and to a decrease in diethyl ether production. Crotonaldehyde is consistent with the formation of 1-butanol as expected, according to the Guerbet route [15, 73, 76, 80–83] (Figure 4 - steps 10, 11, 20, 21). 1,3-Butadiene production occurs at higher temperature (around 873 K), temperature above which both 1-butanol and 1,3-butadiene are produced. At this temperature, the crotonaldehyde quantity is reduced compared to the first peak concomitant to the 1-butanol production. This phenomenon can be explained by a faster dehydration of the crotyl alcohol on zirconia acid sites (i.e., the system prefers to undergo step 13 over step

22, Figure 4) and a simultaneous disturbance of the crotonaldehyde/crotyl alcohol equilibrium. These phenomena would lead to a decrease of the concentration of the intermediate compounds in the mix.

In a different pattern, both 3.5 wt.% Nb_2O_5/ZrO_2 and 10 wt.% SiO_2/ZrO_2 catalysts (Figures 6b and c, respectively) presented simultaneous desorption of 1-butanol and 1,3-butadiene with peaks at 680 K and 688 K. In addition, the production of crotonaldehyde, 1-butanol and 1,3-butadiene started at similar temperatures, around 653 K. This result is consistent with Guerbet and Gorin-Jones reaction pathways, which involve crotonaldehyde as common intermediate [19, 84] (steps 11, 12 and 20 in Figure 4). As both 1-butanol and 1,3-butadiene reaction pathways involve acid-base pair site at the aldol condensation key reaction steps [73, 76, 81], the observed similar behavior of Nb_2O_5/ZrO_2 and SiO_2/ZrO_2 catalysts, whose basic properties are alike, is not surprising. For both catalysts, a maximum production of 1-butanol and 1,3-butadiene seems to take place around 673 K. Regarding the 10 wt.% WO_3/ZrO_2 catalyst (Figure 6d), 1,3-butadiene started to desorb at lower temperature compared to the other catalyst (603 K instead of 683 K for the other catalysts). This lower temperature can be again explained by the greater number of acid sites of the WO_3/ZrO_2, favoring the dehydration reactions of 1,3-butadiene. 1-Butanol desorbed weakly below 623 K, then more significantly above this temperature. This result suggests favorable formation of 1,3-butadiene over 1-butanol, especially at lower temperatures. Nevertheless, above 723 K, 1-butanol production significantly increased while the 1,3-butadiene production decreased. This phenomenon can be ascribed to the deactivation of the acid sites of the catalyst by carbon deposit. Indeed, oxidative TGA of the sample after the catalytic run evidenced a mass loss of 14.1 % between 573 and 773 K for the WO_3/ZrO_2 catalyst, which can be attributed to the oxidation of the carbon deposit (Figure S1). On the contrary, Nb_2O_5/ZrO_2 and SiO_2/ZrO_2 catalysts did not exhibit any significant mass loss.

3.2.2 Catalytic Tests

Catalytic tests were performed between 623 K and 723 K, to further confirm the trends observed on the TPSR. Figure 7 presents ethanol conversion as function of temperature. After running the reaction stepwise at 623 K, 673 K, and 723 K, the temperature of the reactor was decreased back to 623 K to check for possible catalyst deactivation. Conversion significantly increased with temperature, achieving around 90 % at 723 K for all catalysts, except for WO_3/ZrO_2. The latter presented the highest activity

at initial temperatures, with 32 % ethanol conversion at 623 K, while zirconia exhibited 19 % ethanol conversion, SiO_2/ZrO_2 and Nb_2O_5/ZrO_2, 8 and 11 % respectively. At higher temperatures, ZrO_2, SiO_2/ZrO_2 and Nb_2O_5/ZrO_2 presented similar ethanol conversions (around 90 %), while ethanol conversion decreased on the WO_3/ZrO_2 catalyst, surrounding 70 %. Moreover, the reuse of the catalyst for a second run at 623 K evidences a decrease in conversion from 32 % to 18 % over WO_3/ZrO_2. These results are consistent with the deactivation of the catalyst during the reaction. This can be explained by carbon deposition [84], observed by TGA on the catalyst after the catalytic run, as mentioned above (Figure S1). On the other hand, the other catalysts do not exhibit significant loss of activity, which is also consistent with the absence of carbon deposit on TGA. Interestingly, the WO_3/ZrO_2 catalyst, exhibiting high acid site concentration, suffered from similar deactivation than that observed in zeolites [8].

Figure 7. Ethanol conversion versus temperature. Conditions: P = 1 atm; T = 623 K – 723 K; m_{cat} = 40 mg ; F = 80 mL·min (5 % Et/He). Line between points aims to provide a guide for reading but do not represent a model at intermediary temperature.

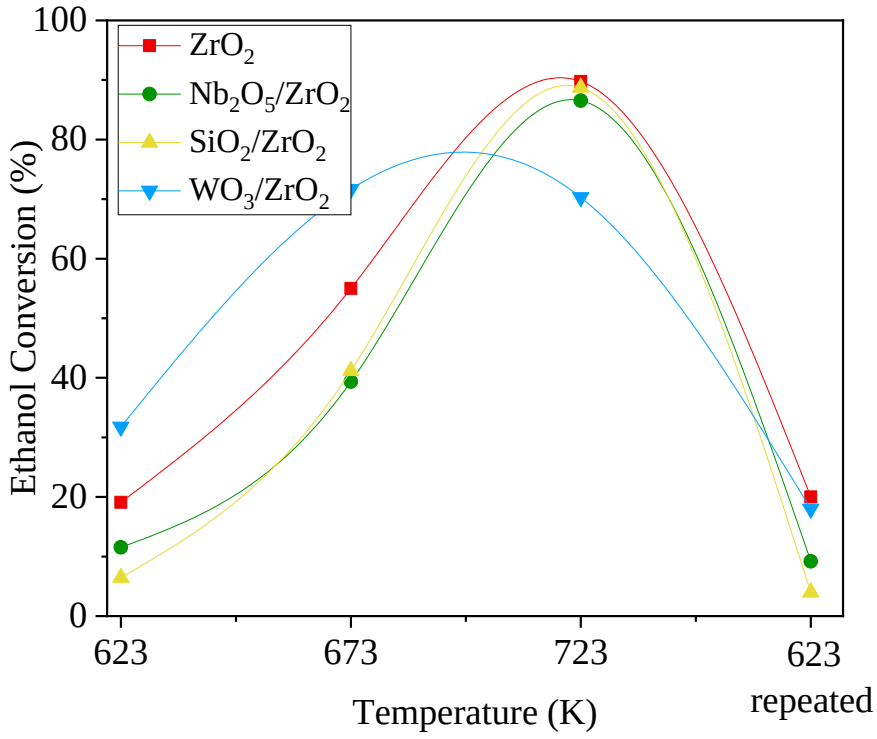

The predominant product obtained for all the catalysts is ethylene (Figure 8), in agreement with the predominance of acid sites evidenced in the NH_3-TPD measurements, which favor ethanol dehydration. The WO_3/ZrO_2 catalyst displayed largest ethanol

conversion and ethylene selectivity (85 %) at 623 K. The trend is reversed at higher temperature due to deactivation. Both the high acidity observed in the NH_3-TPD and the high conversion at low temperatures in the TPSR tests suggest that the WO_3/ZrO_2 catalyst would be the most efficient catalyst for ethanol dehydration. However, although this assumption is correct at the lowest assessed temperature, when conversion rates are still low, the ZrO_2 support appeared as the most efficient catalyst for ethylene dehydration, with 93 % of ethylene selectivity and 55 % of ethanol conversion at 673 K, achieving 90 % of ethanol conversion with the same selectivity towards ethylene at 723 K. Ethanol conversion and selectivity remained similar to those reported by Gao *et al*. over monoclinic zirconia (47 % ethanol conversion and 90 % ethylene selectivity) [21]. Such selectivities and conversion are still less interesting than those exhibited on zeolites, the go-to catalyst for this reaction, which though suffer quick deactivation [8]. In these systems, 99 % ethanol conversion and 99 % selectivity are observed at as low temperature as 513 K [7]. Other metal oxide catalysts are still more efficient than the zirconia, including alumina-derived catalysts, in which 99 % ethanol and 99 % ethylene selectivity could be achieved between 623 K and 713 K [7].

Figure 8 also depicts the selectivities to the other main products as a function of temperature. Detailed selectivities of the obtained products are presented in Table S1. As expected, diethyl ether is produced at lower temperatures and with lower selectivity (maximum 10 % over ZrO_2 at 623 K) [90]. Diethyl ether is obtained by ethanol dehydration over acid sites and competes with ethylene formation. Nevertheless, its formation is favored at lower reaction temperatures. Diethyl ether selectivity decreasing with temperature is consistent with an ethylene and C3-C4 compounds selectivities increasing [70, 76] on the catalysts that did not undergo deactivation. Furthermore, a reverse trend in comparison to the ethylene selectivity was observed in the acetaldehyde selectivity curves (Figure 7 and 8). The less active catalysts towards ethylene dehydration, Nb_2O_5/ZrO_2 and SiO_2/ZrO_2, are those exhibiting the largest acetaldehyde selectivities (Figure 8 b and c), with 12 % and 10 % respectively at 623 K. The more ethylene is produced, the less acetaldehyde is observed. This is consistent with the observation that the dehydration reactions are favored compared to dehydrogenation reactions. These findings are easily noticeable in the selectivity versus ethanol conversion plots (Figures S2-S5). A similar assumption was formulated regarding the dehydration of crotyl alcohol on the TPSR tests. As neither Nb_2O_5, SiO_2 nor WO_3 are known for their redox properties, zirconia is assumedly the main source of redox sites on all catalysts [91–93]. Furthermore,

the addition of Nb_2O_5 and SiO_2 increased acetaldehyde selectivity, leading to 10 % and 12 %, respectively, at 623 K (Figures 8 b and c). Nevertheless, acetaldehyde selectivity also decreased with rising temperature. Temperature increases thus favored ethylene formation instead of acetaldehyde formation by ethanol dehydrogenation. The same results were observed by Da Ros *et al.* [94].

Figure 8. Products selectivities versus temperature. (a) ZrO_2 (b) Nb_2O_5/ZrO_2 (c) SiO_2/ZrO_2 (d) WO_3/ZrO_2. Conditions: P = 1 atm; T = 623 K – 723 K; m_{cat} = 40 mg; F = 80 mL·min (5 % Et/He). Line between points aims to provide a guide for reading but do not represent a model at intermediary temperature.

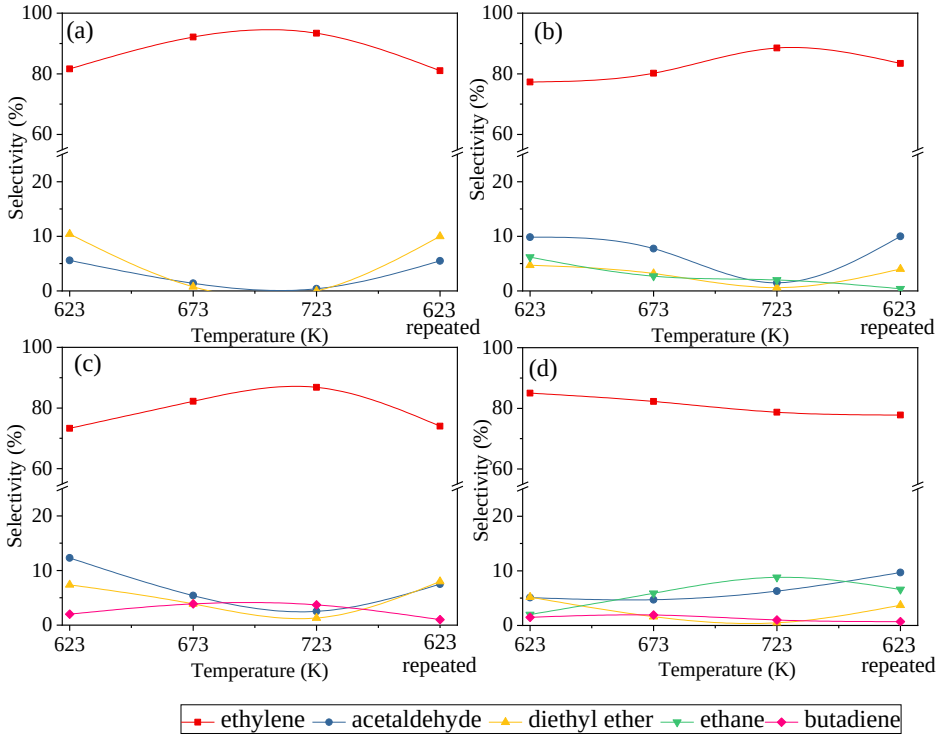

As an intermediate compound, acetaldehyde leads to the formation of 1-butanol, 1,3-butadiene and acetone. Acetone production is also scant. However, the last step of the reaction relies on a ketonization reaction over basic sites [22, 64]. This is consistent with the largest acetone selectivities being obtained over ZrO_2 catalyst (Table S1), which exhibited the largest number of basic sites. Furthermore, over all catalysts, 1-butanol is either not detectable or produced in very low quantities (less than 0.5 %, Figure 8). Consequently, as suggested by the TPSR trends, 1,3-butadiene is favored over 1-butanol, probably due to the quick dehydration step leading to 1,3-butadiene (Figure 4, step 13) compared to the dehydrogenation steps leading to 1-butanol (Figure 4, steps 22 or 20-21). SiO_2/ZrO_2 yielded the highest selectivity towards 1,3-butadiene, around 4 % at 673 K (Figure 8c), which is in agreement with the TPSR results (Figure 6). This catalyst, also

presenting the best selectivities towards acetaldehyde, exhibits an advantageous acid-base balance compared to the other catalysts (Table 2). As the key aldol coupling step requires acid-base pair sites with a pronounced basic character [19], the formation of both 1,3-butadiene and 1-butanol over the SiO_2/ZrO_2 catalyst is not surprising. The results obtained for C3 and C4 compounds are restricted by the limited redox properties of the catalysts, properties here only provided by the zirconia support. This feature is clearly observed for acetaldehyde production, resulting from ethanol dehydrogenation. As acetaldehyde is an intermediate of the acetone, 1-butanol and 1,3-butadiene pathways, the low quantity of redox sites is responsible of the modest results toward C3 and C4 compounds. Even though the selectivity observed over the catalysts in our study is low compared to those reported in the literature (with yield exceeding 80 %) [13, 17], we bring evidences of the particularities of each catalyst. The catalysts described in the literature for 1,3-butadiene synthesis generally rely on a combination of metal oxides among which one of oxides exhibits high redox properties [13, 17, 91]. In particular, a gold-doped SiO_2/ZrO_2 catalyst reached 82 % 1,3-butadiene yield [17]. It should also be noticed that the operational conditions, including contact times [94], have critical impact on the 1,3-butadiene production and are not considered in the present work.

Even if ethane is not the focus of this study due to its low added value, it is noteworthy that ethane was also obtained, reaching more than 8 % at 723 K on the WO_3/ZrO_2 catalyst. Ethane selectivity usually decreases with ethylene production. Traces of propene, 1-butene, ethyl acetate and acetone could also be identified (Supplementary Information Table S1).

4 CONCLUSION

This work studied ethanol conversion on ZrO_2-based catalysts. All catalysts were able to convert 50 % of the ethanol between 543 K and 673 K. Acid-basic properties strongly influence the selectivity of the obtained compounds. Catalysts presenting strong acidity clearly favored the dehydration of ethanol to ethylene, but quickly suffered deactivation by carbon deposition. Unlike it would have been expected, the most acidic catalysts were not the most efficient toward ethylene production. Pure zirconia, exhibiting moderate acidity compared to the other assessed catalysts, achieved the best results with 93 % of ethylene selectivity and 56 % of ethanol conversion at 673 K. C3 to C4 compounds are also formed starting at 673 K. The combination of both basicity and acidity leads to the formation of heavier compounds including acetone, 1,3-butadiene and

1-butanol. In particular, the largest selectivity towards 1,3-butadiene (around 4 %) was obtained on the SiO_2/ZrO_2 catalyst. The moderate results obtained for C3 and C4 compounds can be explained by the limited redox properties of the catalysts only provided here by the zirconia support. In addition, the strong acidic properties of the studied catalysts result in a 1,3-butadiene production favored over 1-butanol. Nonetheless, as acid catalysts are impacted by deactivation, 1,3-butadiene production also suffers from this phenomenon.

Doping the zirconia support by wet impregnation with niobium oxide clearly affected zirconia properties, as it created more acid sites than those observed in the conventional pure zirconia support. Despite an interesting acid-base balance and one of the most interesting acetaldehyde productions observed here, the results toward C3 and C4 compounds were better on other catalysts. It is noteworthy that increasing the proportion of niobium is not expected to dramatically improve the catalyst performances due to a probable increase of acidic properties and consequently of the deactivation phenomenon. The niobia modification favored the formation of heavier compound, and of acetaldehyde, at relatively low temperature (623 K).

Nevertheless, this study suggests that the modification of zirconia enables the reactivity of the catalyst to be tuned. The proportion and strength of both basic and acid sites strongly influence the proportion of heavier products obtained from ethanol and thus favor the production of higher products.

ACKNOWLEDGEMENTS

The authors thank the NORPRO company, provider of some commercial catalysts as well as the CBMM company who provided the niobium salt. The CNPq and the BRAFITEC program are also greatly acknowledged for the funding of F. Lopes and the opportunity of academic exchange of M. Laird respectively.

DECLARATIONS

The authors have no relevant financial or non -financial interests to disclose.

HIGHLIGHTS

- New niobium-doped zirconia catalyst with enhanced acidity was developed.

- Strong acidity favored ethanol dehydration to ethylene, but also increased catalyst deactivation.
- A correlation between acid-base properties and selectivity towards heavier compounds could be observed.
- 1,3-butadiene production was favored against 1-butanol due to the quick dehydration steps over acid sites, but suffered from deactivation by carbon deposit.
- For improved performances toward C3 and C4 compound, redox properties should be enhanced.

REFERENCES

1. Bozell JJ, Petersen GR (2010) Technology development for the production of biobased products from biorefinery carbohydrates—the US Department of Energy's "Top 10" revisited. Green Chem 12:539. https://doi.org/10.1039/b922014c

2. Gallo JMRR, Bueno JMCC, Schuchardt U (2014) Catalytic transformations of ethanol for biorefineries. J Braz Chem Soc 25:2229–2243. https://doi.org/10.5935/0103-5053.20140272

3. Renewable Fuels Association (2019) Markets and Statistics. https://ethanolrfa.org/statistics/. Accessed 29 Oct 2019

4. Sun J, Wang Y (2014) Recent Advances in Catalytic Conversion of Ethanol to Chemicals. ACS Catal 4:1078–1090. https://doi.org/10.1021/cs4011343

5. Fan D, Dai D-JJ, Wu H-SS (2013) Ethylene formation by catalytic dehydration of ethanol with industrial considerations. Materials (Basel) 6:101–115. https://doi.org/10.3390/ma6010101

6. McKetta JJ (1993) Chemical processing handbook. Marcel Dekker, Inc.

7. Zhang M, Yu Y (2013) Dehydration of Ethanol to Ethylene. Ind Eng Chem Res 52:9505–9514. https://doi.org/10.1021/ie401157c

8. Gayubo AG, Alonso A, Valle B, et al (2010) Hydrothermal stability of HZSM-5 catalysts modified with Ni for the transformation of bioethanol into hydrocarbons. Fuel 89:3365–3372. https://doi.org/10.1016/J.FUEL.2010.03.002

9. Angelici C, Weckhuysen BM, Bruijnincx PCA (2013) Chemocatalytic Conversion of Ethanol into Butadiene and Other Bulk Chemicals. ChemSusChem 6:1595–1614. https://doi.org/10.1002/cssc.201300214

10. Iwamoto M (2015) Selective catalytic conversion of bio-ethanol to propene: A review of catalysts and reaction pathways. Catal Today 242:243–248

11. Furumoto Y, Tsunoji N, Ide Y, et al (2012) Conversion of ethanol to propylene over HZSM-5(Ga) co-modified with lanthanum and phosphorous. Appl Catal A Gen 417–418:137–144. https://doi.org/10.1016/j.apcata.2011.12.034

12. Liu C, Sun J, Smith C, Wang Y (2013) A study of $Zn_xZr_yO_z$ mixed oxides for direct conversion of ethanol to isobutene. Appl Catal A Gen 467:91–97

13. Makshina E V., Dusselier M, Janssens W, et al (2014) Review of old chemistry and new catalytic advances in the on-purpose synthesis of butadiene. Chem Soc Rev 43:7917–7953. https://doi.org/10.1039/C4CS00105B

14. Pacheco HP, de Souza EF, Landi SM, et al (2019) Ru Promoted MgO and Al-Modified MgO for Ethanol Upgrading. Top Catal 62:894–907. https://doi.org/10.1007/s11244-019-01177-y

15. De Souza EF, Pacheco HP, Miyake N, et al (2020) Computational and

Experimental Mechanistic Insights into the Ethanol-to-Butanol Upgrading Reaction over MgO. ACS Catal 15162–15177. https://doi.org/10.1021/acscatal.0c04616

16. Prillaman JT, Miyake N, Davis RJ (2021) Calcium Phosphate Catalysts for Ethanol Coupling to Butanol and Butadiene. Catal Letters 151:648–657. https://doi.org/10.1007/s10562-020-03342-5

17. Ezinkwo GO, Tretyakov VP, Aliyu A, Ilolov AM (2014) Fundamental Issues of Catalytic Conversion of Bio-Ethanol into Butadiene. ChemBioEng Rev 1:194–203. https://doi.org/10.1002/cben.201400007

18. Xu Y, Liu Z, Han Z, Zhang M (2017) Ethanol/acetaldehyde conversion into butadiene over sol–gel ZrO_2 –SiO_2 catalysts doped with ZnO. RSC Adv 7:7140–7149. https://doi.org/10.1039/C6RA25139K

19. Makshina EV, Janssens W, Sels BF, Jacobs PA (2012) Catalytic study of the conversion of ethanol into 1,3-butadiene. Catal Today 198:338–344. https://doi.org/10.1016/J.CATTOD.2012.05.031

20. Kyriienko PI, Larina O V., Soloviev SO, et al (2017) Ethanol Conversion into 1,3-Butadiene by the Lebedev Method over MTaSiBEA Zeolites (M = Ag, Cu, Zn). ACS Sustain Chem Eng 5:2075–2083. https://doi.org/10.1021/acssuschemeng.6b01728

21. Gao M, Zhang M, Yu Y (2016) Study on the Reaction Species of 1, 3-Butadiene Formation from Bio-ethanol on ZrO_2. Catal Letters 146:2450–2457. https://doi.org/10.1007/s10562-016-1856-9

22. Rodrigues CP, Zonetti P da C, Appel LG (2017) Chemicals from ethanol: the acetone synthesis from ethanol employing $Ce_{0.75}Zr_{0.25}O_2$, ZrO_2 and $Cu/ZnO/Al_2O_3$. Chem Cent J 11:30. https://doi.org/10.1186/s13065-017-0249-5

23. Xia W, Wang F, Mu X, Chen K (2017) Transformation of ethanol to propylene on ZrO_2 catalysts: effect of reaction conditions on the catalytic performance. React Kinet Mech Catal 122:463–472. https://doi.org/10.1007/s11144-017-1193-z

24. Xia W, Wang F, Mu X, Chen K (2017) Remarkably enhanced selectivity for conversion of ethanol to propylene over ZrO_2 catalysts. Fuel Process Technol 166:140–145. https://doi.org/10.1016/J.FUPROC.2017.06.002

25. Xia W, Wang F, Wang L, et al (2018) High Performance SiO_2–ZrO_2 Binary Oxide for Ethanol Conversion to Ethylene. Catal Letters 148:3024–3034. https://doi.org/10.1007/s10562-018-2500-7

26. Gao M, Jiang H, Zhang M (2018) The influence of calcination temperatures on the acid-based properties and catalytic activity for the 1,3-butadiene synthesis from ethanol/acetaldehyde mixture. Appl Surf Sci 439:1072–1078. https://doi.org/10.1016/J.APSUSC.2018.01.053

27. Onfroy T, Clet G, Houalla M (2005) Correlations between Acidity, Surface Structure, and Catalytic Activity of Niobium Oxide Supported on Zirconia. J Phys Chem B 109:14588–14594. https://doi.org/10.1021/jp0517347

28. Phung TK, Proietti Hernández L, Busca G (2015) Conversion of ethanol over transition metal oxide catalysts: Effect of tungsta addition on catalytic behaviour of titania and zirconia. Appl Catal A Gen 489:180–187. https://doi.org/10.1016/j.apcata.2014.10.025

29. Dancini-Pontes I, DeSouza M, Silva FA, et al (2015) Influence of the CeO_2 and Nb_2O_5 supports and the inert gas in ethanol steam reforming for H2 production. Chem Eng J 273:66–74. https://doi.org/10.1016/J.CEJ.2015.03.032

30. Alonso CG, Furtado AC, Cantão MP, et al (2009) Reactions over Cu/Nb_2O_5 catalysts promoted with Pd and Ru during hydrogen production from ethanol. Int J Hydrogen Energy 34:3333–3341. https://doi.org/10.1016/J.IJHYDENE.2009.02.021

31. Asakura K, Iwasawa Y (1986) The surface structure and catalytic properties of one-atomic layer amorphous niobium-oxide attached on SiO_2. Chem Lett 15:859–862. https://doi.org/10.1246/cl.1986.859

32. Brandão P, Philippou A, Rocha J, Anderson MW (2002) Dehydration of Alcohols by Microporous Niobium Silicate AM-11. Catal Letters 80:99–102. https://doi.org/10.1023/A:1015444005961

33. Zhu H, Chaudhari R V., Subramaniam B, et al (2017) Effects of tunable acidity and basicity of Nb-KIT-6 catalysts on ethanol conversion: Experiments and kinetic modeling. AIChE J 63:2888–2899. https://doi.org/10.1002/aic.15648

34. Anastas P, Eghbali N (2009) Green Chemistry: Principles and Practice. Chem Soc Rev 39:301–312. https://doi.org/10.1039/B918763B

35. Annual U.S. & World Fuel Ethanol Production | Renewable Fuels Association. https://ethanolrfa.org/statistics/annual-ethanol-production/. Accessed 23 Aug 2021

36. Survey USG (2021) Mineral commodity summaries 2021. Miner Commod Summ. https://doi.org/10.3133/MCS2021

37. Chagas LH, Matheus CRV, Zonetti PC, Appel LG (2018) Butadiene from ethanol employing doped t-ZrO_2. Mol Catal 458:272–279. https://doi.org/10.1016/j.mcat.2018.01.018

38. Zonetti PC, Celnik J, Letichevsky S, et al (2011) Chemicals from ethanol – The dehydrogenative route of the ethyl acetate one-pot synthesis. J Mol Catal A Chem 334:29–34. https://doi.org/10.1016/j.molcata.2010.10.019

39. De Lima AFF, Zonetti PC, Rodrigues CP, Appel LG (2017) The first step of the propylene generation from renewable raw material: Acetone from ethanol employing CeO_2 doped by Ag. Catal Today 279:252–259. https://doi.org/10.1016/j.cattod.2016.04.038

40. González Vargas OA, de Los Reyes Heredia JA, Suarez-Toriello VA, et al (2021) Enhanced catalytic performance of Ce-MCM-41-supported Rh for CO oxidation. Res Chem Intermed 2021 477 47:2857–2880. https://doi.org/10.1007/S11164-021-04436-4

41. Ko EI, Weissman JG (1990) Structures of niobium pentoxide and their

implications on chemical behavior. Catal Today 8:27–36. https://doi.org/10.1016/0920-5861(90)87005-N

42. Larina O, Kyriienko P, Soloviev S (2015) Ethanol Conversion to 1,3-Butadiene on ZnO/MgO–SiO2 Catalysts: Effect of ZnO Content and MgO:SiO_2 Ratio. Catal Letters 145:1162–1168. https://doi.org/10.1007/s10562-015-1509-4

43. Onfroy T, Clet G, Houalla M (2005) Acidity, Surface Structure, and Catalytic Performance of WO_x Supported on Monoclinic Zirconia. J Phys Chem B 109:3345–3354. https://doi.org/10.1021/jp048435m

44. Busca G (2014) Heterogeneous catalytic materials : solid state chemistry, surface chemistry and catalytic behaviour, Elsevier

45. Watanabe M, Aizawa Y, Iida T, et al (2005) Catalytic glucose and fructose conversions with TiO_2 and ZrO_2 in water at 473 K: Relationship between reactivity and acid-base property determined by TPD measurement. Appl Catal A Gen 295:150–156. https://doi.org/10.1016/j.apcata.2005.08.007

46. Manríquez M, López T, Gómez R, Navarrete J (2004) Preparation of TiO_2-ZrO_2 mixed oxides with controlled acid-basic properties. J Mol Catal A Chem 220:229–237. https://doi.org/10.1016/j.molcata.2004.06.003

47. Bosman HJM, Kruissink EC, Van der spoel J, Van den Brink F (1994) Characterization of the acid strength of SiO_2-ZrO_2 mixed oxides. J Catal 148:660–672. https://doi.org/10.1006/jcat.1994.1253

48. Dang Z, Anderson BG, Amenomiya Y, Morrow BA (1995) Silica-supported zirconia. 1. Characterization by infrared spectroscopy, temperature-programmed desorption, and X-ray diffraction. J Phys Chem 99:14437–14443. https://doi.org/10.1021/j100039a036

49. Ramanathan A, Maheswari R, Barich DH, Subramaniam B (2014) Niobium incorporated mesoporous silicate, Nb-KIT-6: Synthesis and characterization. Microporous Mesoporous Mater 190:240–247. https://doi.org/10.1016/j.micromeso.2014.02.019

50. Heracleous E, Lemonidou AA (2006) Ni-Nb-O mixed oxides as highly active and selective catalysts for ethene production via ethane oxidative dehydrogenation. Part I: Characterization and catalytic performance. J Catal 237:162–174. https://doi.org/10.1016/j.jcat.2005.11.002

51. Yang P, Fan S, Chen Z, et al (2018) Synthesis of Nb_2O_5 based solid superacid materials for catalytic combustion of chlorinated VOCs. Appl Catal B Environ 239:114–124. https://doi.org/10.1016/j.apcatb.2018.07.061

52. García-Sancho C, Cecilia JA, Moreno-Ruiz A, et al (2015) Influence of the niobium supported species on the catalytic dehydration of glycerol to acrolein. Appl Catal B Environ 179:139–149. https://doi.org/10.1016/j.apcatb.2015.05.014

53. Nowak I, Ziolek M (1999) Niobium Compounds: Preparation, Characterization, and Application in Heterogeneous Catalysis. Chem Rev 99:3603–3624.

https://doi.org/10.1021/cr9800208

54. Onfroy T, Clet G, Bukallah SB, et al (2003) Development of the Acidity of Zirconia-Supported Niobia Catalysts. Catal Letters 89:15–19. https://doi.org/10.1023/A:1024717505705

55. Onfroy T, Clet G, Bukallah SB, et al (2006) Acidity of titania-supported tungsten or niobium oxide catalysts: Correlation with catalytic activity. Appl Catal A Gen 298:80–87. https://doi.org/10.1016/J.APCATA.2005.09.021

56. Witoon T, Chalorngtham J, Dumrongbunditkul P, et al (2016) CO_2 hydrogenation to methanol over Cu/ZrO_2 catalysts: Effects of zirconia phases. Chem Eng J 293:327–336. https://doi.org/10.1016/j.cej.2016.02.069

57. Onfroy T, Clet G, Houalla M (2001) Development of acidic sites in WO_x/ZrO_2. Chem Commun 0:1378–1379. https://doi.org/10.1039/b102867g

58. Weingarten R, Tompsett GA, Conner WC, Huber GW (2011) Design of solid acid catalysts for aqueous-phase dehydration of carbohydrates: The role of Lewis and Brønsted acid sites. J Catal 279:174–182. https://doi.org/10.1016/j.jcat.2011.01.013

59. Gervasini A, Auroux A (1991) Acidity and basicity of metal oxide surfaces II. Determination by catalytic decomposition of isopropanol. J Catal 131:190–198. https://doi.org/10.1016/0021-9517(91)90335-2

60. Yan H, Yang Y, Tong D, et al (2009) Catalytic conversion of glucose to 5-hydroxymethylfurfural over SO_4^{2-}/ZrO_2 and SO_4^{2-}/ZrO_2-Al_2O_3 solid acid catalysts. Catal Commun 10:1558–1563. https://doi.org/10.1016/j.catcom.2009.04.020

61. Sánchez-Sánchez MC, Navarro RM, Fierro JLG (2007) Ethanol steam reforming over Ni / M_xO_y-Al_2O_3 (M = Ce, La, Zr and Mg) catalysts: Influence of support on the hydrogen production. Int J Hydrogen Energy 32:1462–1471. https://doi.org/10.1016/j.ijhydene.2006.10.025

62. Chen WH, Ko HH, Sakthivel A, et al (2006) A solid-state NMR, FT-IR and TPD study on acid properties of sulfated and metal-promoted zirconia: Influence of promoter and sulfation treatment. Catal Today 116:111–120. https://doi.org/10.1016/j.cattod.2006.01.025

63. Chen L, Zhu Y, Zheng H, et al (2011) Aqueous-phase hydrodeoxygenation of carboxylic acids to alcohols or alkanes over supported Ru catalysts. J Mol Catal A Chem 351:217–227. https://doi.org/10.1016/j.molcata.2011.10.015

64. Rodrigues CP, Zonetti PC, Silva CG, et al (2013) Chemicals from ethanol—The acetone one-pot synthesis. Appl Catal A Gen 458:111–118. https://doi.org/10.1016/J.APCATA.2013.03.028

65. Li Y, He D, Ge S, et al (2008) Effects of CO_2 on synthesis of isobutene and isobutane from $CO_2/CO/H_2$ reactant mixtures over zirconia-based catalysts. Appl Catal B Environ 80:72–80. https://doi.org/10.1016/J.APCATB.2007.11.004

66. Sung KH, Cheng S (2017) Effect of Nb doping in WO3/ZrO2 catalysts on gas

phase dehydration of glycerol to form acrolein. RSC Adv 7:41880–41888. https://doi.org/10.1039/c7ra08154e

67. Lee EJ, Lee J, Lee M, et al (2019) Propylene epoxidation by oxygen over tungsten oxide supported on ceria-zirconia. Mol Catal 467:111–119. https://doi.org/10.1016/j.mcat.2019.02.001

68. Phongamwong T, Chantaprasertporn U, Witoon T, et al (2017) CO_2 hydrogenation to methanol over CuO–ZnO–ZrO_2–SiO_2 catalysts: Effects of SiO_2 contents. Chem Eng J 316:692–703. https://doi.org/10.1016/j.cej.2017.02.010

69. Arena F, Italiano G, Barbera K, et al (2008) Solid-state interactions, adsorption sites and functionality of Cu-ZnO/ZrO_2 catalysts in the CO_2 hydrogenation to CH_3OH. Appl Catal A Gen 350:16–23. https://doi.org/10.1016/j.apcata.2008.07.028

70. Phung TK, Busca G (2015) Ethanol dehydration on silica-aluminas: Active sites and ethylene/diethyl ether selectivities. Catal Commun 68:110–115. https://doi.org/10.1016/J.CATCOM.2015.05.009

71. Phung TK, Busca G (2015) Diethyl ether cracking and ethanol dehydration: Acid catalysis and reaction paths. Chem Eng J 272:92–101. https://doi.org/10.1016/J.CEJ.2015.03.008

72. Christiansen MA, Mpourmpakis G, Vlachos DG (2015) DFT-driven multi-site microkinetic modeling of ethanol conversion to ethylene and diethyl ether on γ-Al2O3(1 1 1). J Catal 323:121–131. https://doi.org/10.1016/J.JCAT.2014.12.024

73. Dai J, Zhang H (2019) Recent advances in selective C-C bond coupling for ethanol upgrading over balanced Lewis acid-base catalysts. Sci. China Mater. 62:1642–1654

74. Dussol D, Cadran N, Laloue N, et al (2019) New insights of butadiene production from ethanol: Elucidation of concurrent reaction pathways and kinetic study. Chem Eng J 123586. https://doi.org/10.1016/j.cej.2019.123586

75. Jones MD, Keir CG, Iulio C Di, et al (2011) Investigations into the conversion of ethanol into 1,3-butadiene. Catal Sci Technol 1:267–272. https://doi.org/10.1039/c0cy00081g

76. Di Cosimo JI, Díez VK, Xu M, et al (1998) Structure and Surface and Catalytic Properties of Mg-Al Basic Oxides. J Catal 178:499–510. https://doi.org/10.1006/JCAT.1998.2161

77. Yang C, Meng ZY (1993) Bimolecular condensation of ethanol to 1-Butanol catalyzed by alkali cation zeolites. J Catal 142:37–44. https://doi.org/10.1006/jcat.1993.1187

78. Bi JL, Hong YY, Lee CC, et al (2007) Novel zirconia-supported catalysts for low-temperature oxidative steam reforming of ethanol. Catal Today 129:322–329. https://doi.org/10.1016/j.cattod.2006.11.027

79. Ndou AS, Plint N, Coville NJ (2003) Dimerisation of ethanol to butanol over solid-base catalysts. Appl Catal A Gen 251:337–345. https://doi.org/10.1016/S0926-

860X(03)00363-6

80. Scalbert J, Thibault-Starzyk F, Jacquot R, et al (2014) Ethanol condensation to butanol at high temperatures over a basic heterogeneous catalyst: How relevant is acetaldehyde self-aldolization? J Catal 311:28–32. https://doi.org/10.1016/J.JCAT.2013.11.004

81. Di Cosimo JI, Apesteguia CR, Ginés MJL, Iglesia E (2000) Structural Requirements and Reaction Pathways in Condensation Reactions of Alcohols on Mg_yAlO_x Catalysts. J Catal 190:261–275. https://doi.org/10.1006/JCAT.1999.2734

82. Carvalho DL, de Avillez RR, Rodrigues MT, et al (2012) Mg and Al mixed oxides and the synthesis of n-butanol from ethanol. Appl Catal A Gen 415–416:96–100. https://doi.org/10.1016/J.APCATA.2011.12.009

83. Carvalho DL, Borges LEP, Appel LG, et al (2013) In situ infrared spectroscopic study of the reaction pathway of the direct synthesis of n-butanol from ethanol over MgAl mixed-oxide catalysts. Catal Today 213:115–121. https://doi.org/10.1016/J.CATTOD.2013.03.034

84. Tsuchida T, Kubo J, Yoshioka T, et al (2008) Reaction of ethanol over hydroxyapatite affected by Ca/P ratio of catalyst. J Catal 259:183–189. https://doi.org/10.1016/J.JCAT.2008.08.005

85. Young ZD, Davis RJ (2018) Hydrogen transfer reactions relevant to Guerbet coupling of alcohols over hydroxyapatite and magnesium oxide catalysts. Catal Sci Technol 8:1722–1729. https://doi.org/10.1039/c7cy01393k

86. Lewandowski M, Babu GS, Vezzoli M, et al (2014) Investigations into the conversion of ethanol to 1,3-butadiene using $MgO:SiO_2$ supported catalysts. Catal Commun 49:25–28. https://doi.org/10.1016/J.CATCOM.2014.02.003

87. Inoue R, Ichikawa A, Furukawa K (1958) Synthesis of Butadiene from 4-Oxy-2-butanone and Alcohol. J Soc Chem Ind Japan 61:566–569. https://doi.org/10.1246/nikkashi1898.61.566

88. Silva-Calpa L del R, Zonetti PC, Rodrigues CP, et al (2016) The $Zn_xZr_{1-x}O_{2-y}$ solid solution on m-ZrO_2: Creating O vacancies and improving the m-ZrO_2 redox properties. J Mol Catal A Chem 425:166–173. https://doi.org/10.1016/j.molcata.2016.10.008

89. Liguras DK, Goundani K, Verykios XE (2004) Production of hydrogen for fuel cells by catalytic partial oxidation of ethanol over structured Ni catalysts. J Power Sources 130:30–37. https://doi.org/10.1016/j.jpowsour.2003.12.008

90. Madeira FF, Gnep NS, Magnoux P, et al (2009) Ethanol transformation over HFAU, HBEA and HMFI zeolites presenting similar Brønsted acidity. Appl Catal A Gen 367:39–46. https://doi.org/10.1016/J.APCATA.2009.07.033

91. Badlani M, Wachs IE (2001) Methanol: A “smart” chemical probe molecule. Catal Letters 75:137–149. https://doi.org/10.1023/A:1016715520904

92. Kulkarni D, Wachs IE (2002) Isopropanol oxidation by pure metal oxide catalysts: Number of active surface sites and turnover frequencies. Appl Catal A Gen 237:121–137. https://doi.org/10.1016/S0926-860X(02)00325-3

93. Deo G, Wachs IE (1994) Reactivity of Supported Vanadium Oxide Catalysts: The Partial Oxidation of Methanol. J Catal 146:323–334. https://doi.org/10.1006/jcat.1994.1071

94. Da Ros S, Jones MD, Mattia D, et al (2017) Modelling the effects of reaction temperature and flow rate on the conversion of ethanol to 1,3-butadiene. Appl Catal A Gen 530:37–47. https://doi.org/10.1016/J.APCATA.2016.11.008